A ruthenium(II) trithiacyclononane curcuminate complex: synthesis, characterisation, DNA interaction and cytotoxic activity

SCHOLARONE™
Manuscripts

1
2
3
4
5
6
7
8
9
10
11
12
13
14
15
16
17
18
19
20
21
22
23
24
25
26
27
28
29
30
31
32
33
34
35
36
37
38
39
40
41
42
43
44
45
46
47
48
49
50
51
52
53
54
55
56
57
58
59
60

Unable to Convert Image

The dimensions of this image (in pixels) are too large
to be converted. For this image to convert,
the total number of pixels (height × width) must be
less than 40,000,000 (40 megapixels).

A ruthenium(II) trithiacyclononane curcuminate complex: synthesis, characterisation, DNA interaction and cytotoxic activity

Magda Carvalho Henriques[a], Maria Amparo F. Faustino[a], Artur M. S. Silva[a], Juliana Felgueiras[b], Margarida Fardilha[b], and Susana Santos Braga[a]*

[a] Department of Chemistry, QOPNA research unit, University of Aveiro, 3810-193 Aveiro, Portugal.

[b] Laboratory of Signal Transduction, Institute for Research in Biomedicine, Medical Sciences Department, University of Aveiro, 3810-193 Aveiro, Portugal.

* Corresponding author: Susana Santos Braga, sbraga@ua.pt

Competing Interests

The authors have no potential conflict of interest to report.

1

A ruthenium(II) trithiacyclononane curcuminate complex: synthesis, characterisation, DNA interaction and cytotoxic activity

The coordination of inorganic ruthenium(II) complexes to anionic oxygen-based donors is very rare. In this study, the simple, one-pot preparation of [ruthenium(II)(trithiacyclononane)(curcumin)(*S*-DMSO)]Cl (**1**) and its structural characterisation by elemental analysis, FT-IR, 1-D and 2-D NMR, ESI[+]-MS as well as UV-VIS and fluorescence are described. DNA thermal degradation studies showed that the complex **1** has DNA-intercalating ability, while pure curcumin is a non-intercalative compound. The *in vitro* cytotoxic activity of the complex **1**, in comparison with that of pure curcumin, was investigated using the tumor human prostate cell line, PC-3, and the pre-neoplastic cell line, PNT-2. Results showed that complex **1** is innocuous towards normal prostate epithelial cells and, whereas curcumin is toxic in concentrations of 50 and 80 μM. On the tumour cell line PC-3, the complex **1** did not cause viability changes whereas curcumin exhibited dose-dependent inhibition. This study suggests that coordination with the trithiacyclononane ruthenium(II) scaffold stabilises the photochemical properties and biologic activity of curcumin.

Keywords: Curcumin; Ruthenium complexes; Spectroscopic characterisation; DNA intercalation; Cytotoxicity.

1. Introduction

Curcumin is a yellow pigment obtained from the dried rhizome of the plant *Curcuma longa* L., isolated for the first time in 1815 [1]. It is a molecule capable of modulating many cell signalling pathways, thus possessing a wide range of biological properties that include anti-inflammatory [2,3], antioxidant [4–7] and antitumor [8–11] activities. Curcumin is capable of inducing apoptosis in tumour cells and it contributes to reduction of angiogenesis at tumour sites [12]. However, its absorption rate at the intestine is quite low and it suffers from extensive inactivation due to hepatic first-pass metabolism, resulting in poor bioavailability [13].

In recent years, many solutions were made available for circumventing the low bioavailability of curcumin, from simple formulation strategies to the synthesis of new derivatives and prodrugs [14]. A useful strategy is the coordination of curcumin to a suitable metallic precursor to help increase the solubility and stability in physiological media [15, 16]. Curcumin is known to form complexes with halogenates of zinc(II) [16–18], iron(III) [19], copper(II) [20, 21], palladium(II) [22] and vanadium, with vanadyl bis(acetoacetonate), $VO(acac)_2$ [23]. Curcumin zinc(II) complexes, with dinonyl-2,2'-bipyridine (bpy-9) and 4,4'-bis(hydroxymethyl)-2,2'-bipyridine as spectator ligands, presented antitumor activity on several prostate cancer and neuroblastoma human cell lines, with IC_{50} values at 72 h of incubation in the micromolar range (12-37 μM) [17, 18]. Curcumin palladium complexes active against several colon cancer cell lines (IC_{50} values in the 10-34 μM range) were also reported [24]. Ruthenium complexes are particularly useful for fine-tuned anticancer action, since they are not toxic and some are quite selective for cancer cells, likely due to the ability of ruthenium to mimic iron in binding to biomolecules [25]. Several organometallic ruthenium(II)arene complexes of curcumin were reported [25–27]. The results of the cytotoxic studies on these complexes proved them effective against several human cancer cell lines with significantly lower toxicity on non-tumor cell lines. Of these, the most promising were Ru(hexamethylbenzene)(curcumin)(PTA) and Ru(*p*-cymene)(curcumin)(PTA) (PTA = 1,3,5-triaza-7-phospha-adamantane), which were able to inhibit both cisplatin-sensitive and cisplatin-resistant breast cancer cells of the A2780 line at sub-micromolar concentrations [28]. Their IC_{50} were around 0.4 μM, approximately ten times lower than pure curcumin (IC_{50} 4.3 μM). Their safety, evaluated on a healthy embryonic kidney cell line, HEK293, was relatively high, with IC_{50} values of 4.3 μM and 9.1 μM, respectively.

3

The present paper reports the simple, one-pot synthesis of a new Ru(II)curcumin complex bearing trithiacyclononane ([9]aneS$_3$) as the face-capping ligand in place of the abovementioned arene ligands. Curcumin acts as an *O,O'*- donor ligand, forming a five-member heterocyclic ring containing the Ru(II) atom. The DNA-binding ability and *in vitro* cytotoxic activity against human prostate cell lines (PC-3 and PNT-2) of the new complex was studied, using curcumin as reference.

2. Experimental

2.1. Chemicals

Sodium methoxide (95%) and low molecular weight salmon sperm deoxyribonucleic acid (*sm*DNA) were acquired from Sigma Aldrich.

[Ru(II)([9]aneS$_3$)(*S*-DMSO)Cl$_2$] was prepared according to the procedures described in our previous work [29–33]. Curcumin was extracted and purified from dry turmeric powder using an adaptation of the method described by Revathy et al. [34] (for more details, refer to the electronic supplementary information, section S1).

Solvents were at least of analytical grade and used without further purification.

2.2. Instrumentation

^{1}H and ^{13}C nuclear magnetic resonance (NMR) spectra were recorded on a Bruker Avance 300 spectrometer at 300.13 MHz and 75.47 MHz, respectively, at room temperature. Unequivocal ^{1}H and ^{13}C assignments were made using 2D homonuclear correlation spectroscopy (COSY, ^{1}H,^{1}H), while ^{13}C assignments were made based on 2D heteronuclear single quantum coherence spectroscopy (HSQC, ^{1}H,^{13}C), and heteronuclear multiple bond correlation (HMBC, delay for long-range $J_{C/H}$ couplings were optimised for 7 Hz) experiments. Deuterochloroform (CDCl$_3$) was used as solvent

4

(^{1}H δ 7.26 ppm and ^{13}C δ 77.03 ppm) and tetramethylsilane (TMS) as internal reference.

Chemical shifts are quoted in parts per million (ppm) and the coupling constants (*J*) in

Hertz (Hz).

Fourier-transform infrared (FT-IR) spectra, in the range of 4000-380 cm^{-1}, were

collected as KBr pellets using a Unican Mattson Mod 7000 FTIR spectrophotometer by

averaging 64 scans at a maximum resolution of 2 cm^{-1}. In a typical preparation, 2 mg of

sample were mixed in a mortar with 200 mg of KBr (Sigma-Aldrich, ≥ 99%).

Mass spectra were recorded by C. Barros on a Micromass® Q-TOF 2 mass

spectrometer using methanol as solvent and electrospray ionisation (ESI$^+$-MS). The *m/z*

ratios presented in the characterisation data of the sample are monoisotopic, calculated

using the mass of the most abundant natural isotope of each element (^{1}H, ^{12}C, ^{14}N, ^{16}O,

^{32}S, ^{35}Cl and ^{102}Ru).

Ultraviolet-visible (UV-Vis) solution spectra, used for determine the maximum

of absorption of each compound, were obtained at 25 ℃, using 1 × 1 cm quartz optical

cells and recorded on a Shimadzu UV-2501 PC spectrophotometer using

dimethylformamide (DMF) as solvent. Molar absorptivity of each compound was

determined in concentrations range where Beer-Lambert law is valid. The fluorescence

spectra were recorded using a Horiba Jobin-Yvon FluoroMax-3 spectrofluorimeter.

Elemental analysis for CHNS was performed by M. Marques in a TruSpec 630-

200-200 CHNS Analyser.

The absorbance at 260 nm of *sm*DNA in presence or absence of the complex **1**

were performed on a GBC Cintra 500 UV-Vis spectrophotometer equipped with a

temperature controller (GBC Thermocell).

Cell optical density was measured at 540 and 630 nm using a Tecan Inifinite®

200 PRO-series microplate reader.

5

2.3. Synthesis of [Ru(II)([9]aneS₃)(curcumin)(S-DMSO)]Cl (1)

A solution of curcumin (67.0 mg, 0.182 mmol) in methanol (20 mL) was treated with

sodium methoxide (9.83 mg, 0.182 mmol). The solution was stirred and refluxed under

a nitrogen atmosphere until the colour changed from saffron yellow to dark red (*ca*. 30

min), indicating deprotonation of curcumin. After the change in colour, a methanol (20

mL) solution of [Ru([9]aneS₃)(*S*-DMSO)Cl₂] (62.5 mg, 0.182 mmol) was added to the

reaction vessel and the mixture allowed to reflux for 24 h (Scheme 1). It was then

cooled to room temperature under rest, for c.a. 30 min, and the methanol was

evaporated to near dryness. It was then added diethyl ether (~5 mL) and kept at 4 ºC for

three days to obtain a microcrystalline dark red precipitate. The precipitate was isolated

using a Willstätter filter, washed with diethyl ether (~15 mL), and vacuum-dried (49.1

mg, 37% yield).

Elemental analysis for [Ru(C₆H₁₂S₃)(C₂₁H₁₉O₆)(C₂H₆SO)]Cl·(NaCl)·2(H₂O)

(Mr = 856.01) calculated: C, 40.65; H, 4.80; S, 14.95. Found: C, 39.97; H, 4.90; S,

15.30%.

FT-IR ν(tilde) = 3400 m, 2925 m, 2852 w, 1618 m, 1601 m, 1508 vs, 1505 vs,

1452 s, 1425 s, 1410 s, 1397 s, 1384 s, 1280 m, 1226 m, 1163 m, 1124 m, 1078 m, 1017

m, 986 m, 973 m, 906 w, 823 m, 721 vw, 681 w, 641 vw, 610 vw, 594 vw, 576 vw, 556

w, 554 w, 529 w, 482 w, 454 w, 425 w, 390 vw, 386 vw, 303 vw, 291 vw, 284 vw.

ESI⁺-MS *m/z* (relative intensity %): 727 ([Ru([9]aneS₃)(curc)(*S*-DMSO)]⁺,

100%); 621 ([Ru([9]aneS₃–CH₂CH₂)(curc)]⁺, 56%).

¹H NMR (300.13 MHz, CDCl₃): δ (ppm) 7.30 (2H, d, *J* 16.7 Hz, H-4,4'), 7.10

(2H, dd, *J* 1.8 and 8.3 Hz, H-10,10'), 7.01 (2H, d, *J* 1.8 Hz, H-6,6'), 6.94 (2H, d, *J* 8.3

Hz, H-9,9'), 6.49 (2H, d, *J* 16.7 Hz, H-3,3'), 5.64 (1H, s, H-1) 3.96 (6H, s, 7,7'-OCH₃),

6

2.96 (6H, s, S-CH$_3$), 3.66-3.58, 3.42-3.38, 2.93-2.80, 2.72-2.65 (12H, m, CH$_2$ of

trithiacyclononane).

^{13}C NMR (75.47 MHz, CDCl$_3$): δ (ppm) 178.3 (C-2,2'), 148.6 (C-8,8'), 147.5

(C-7,7'), 138.0 (C-4,4'), 129.2 (C-5,5'), 124.5 (C-3,3'), 121.9 (C-10,10'), 115.4

(C-9,9'), 110.4 (C-6,6'), 102.2 (C-1), 55.1 (7,7'-OCH$_3$), 42.2 (SO(CH$_3$)$_2$), 33.6, 32.1,

29.5 (CH$_2$ of trithiacyclononane).

UV-Vis (DMF): λ$_{max}$ (log ε) = 412 nm (4.51).

2.4. Fluorescence quantum yield

The fluorescence spectra of the complex **1** and curcumin in DMF were measured in

1 × 1 cm quartz optical cells under normal air conditions. The fluorescence quantum

yields (Φ$_F$) were calculated by comparison of the area below the corrected emission

spectrum (450–800 nm) with that of 5,10,15,20-tetraphenylporphyrin (TPP). The TPP

is used as fluorescence standard, having a Φ$_F$ = 0.12 in DMF when operating at λ$_{exc}$ =

430 nm with a 5 nm slit [35]. In all cases, the absorbance of the sample and standard

solutions was kept at 0.02 at the 430 nm (the excitation wavelength). The fluorescence

quantum yield is calculated according to the equation (1):

$$\Phi_F^{sample} = \Phi_F^{ref} \frac{AUC^{sample}(1-10^{-Abs_{ref}})}{AUC^{ref}(1-10^{-Abs_{sample}})} \tag{1}$$

where

- AUC is the integrated area under the fluorescence curves of each compound and
  the reference;

- Abs is the absorbance of the samples and the reference at the excitation
  wavelength.

7

2.5. Photooxidation of 9,10-dimethylanthracene

The ability of the complex **1** and curcumin to generate singlet oxygen was evaluated by

monitoring the photooxidation of 9,10-dimethylanthracene, a singlet oxygen quencher

[36,37]. Solutions of **1** or curcumin in DMF (Abs_{430} ~ 0.10) were aerobic irradiated in

quartz cuvettes with monochromatic light ($\lambda = 430$ nm) in the presence of DMA (30

μM). TPP was used as reference ($\Phi_\Delta = 0.65$) [38]. The kinetics of DMA photooxidation

was studied by following the decrease in its absorbance at 378 nm and the result

registered in a first order plot for the photooxidation of DMA photosensitised by **1**,

curcumin and TPP in DMF. The kinetics of DMA photooxidation in the absence of any

compound was also studied and no significant photodegradation was observed under

irradiation at 430 nm in DMF. The results are expressed as a mean and standard

deviation obtained from three independent experiments.

2.5. DNA denaturation temperature assay

The thermal denaturation temperature of *sm*DNA and of the mixture **1**/*sm*DNA (1 : 10)

was determined in a 10mM phosphate buffer saline solution (PBS, composition

Na_2HPO_4/NaH_2PO_4 in ultrapure water, pH 7.4) containing 1.5×10^{-4} M of *sm*DNA and

1.5×10^{-5} M of complex **1**. Melting curves were recorded at 260 nm with samples being

heated in steps of *ca.* 5 ℃ with 10 min interval between each step. For each temperature

point, three absorbance readings were collected and these were averaged before

plotting. The melting temperature is defined as the temperature at which 50% of the

DNA denaturates into a single strand, and it is obtained from the middle point of the

melting curve (represented in the figure 6). Experimental ΔT_m values were estimated to

be accurate within ± 1 ℃.

8

The concentration of the stock solution of *sm*DNA (prepared by dissolution of 5.13×10^{-7} g in 5 mL of PBS) was determined by spectrophotometry, using the molar extinction coefficient $\varepsilon_{260\ nm}$ 6600 M^{-1} cm^{-1} [39], to afford a value of [DNA] = 356 M. Furthermore, this solution gave a ratio of UV absorbance at A_{260nm}/A_{280nm} of *ca.* 1.90, indicating that *sm*DNA was sufficiently free of protein [40].

2.7. Cytotoxicity assays

In this study, two human prostate cell lines were used: PNT-2 (normal cell line), kindly given by Dr. Ricardo Perez-Tomás (University of Barcelona, Spain) and PC-3 (neoplastic androgen-independent cell line), kindly given by Dr. Rui Medeiros (University of Porto, Portugal). Cells were cultured in Roswell Park Memorial Institute media (RPMI)-1640, supplemented with 10% FBS and 1% penicillin/streptomycin mixture, and maintained in a humidified atmosphere at 37 ºC containing 5% CO_2. Cells having a narrow range of passage number were used for all experiments. Fresh stock solutions of curcumin and complex **1** were prepared in DMSO and protected from light. Further dilutions of these stock solutions were made in RPMI-1640, keeping only 1% of DMSO, to obtain the final concentrations required for the biological assays.

The cytotoxicity of curcumin and complex **1** was determined using the AlamarBlue (AB) assay. This assay is based on the ability of resazurin (blue, non-fluorescent) to change colour in a reducing environment to form the pink-coloured, fluorescent resorufin. It is widely used to monitor cellular health, since resazurin reduction may represent an impairment of the cellular metabolism, an interruption of electron transport or a mitochondrial dysfunction [41]. When added to cell cultures, the oxidised form of the AB is converted to the reduced form by mitochondrial enzymes. This redox reaction is accompanied by a shift in colour of the culture media from blue to pink, which can be easily measured by colorimetric reading at 570 and 630 nm.

9

Cells were seeded in 96-well plates (100 μL per well) at an average density of 5000 cells per well and incubated at 37 ºC for 24 h to allow them to adhere. Curcumin and complex **1**, at concentrations of 20, 50 and 80 μM were added. The treated cells were incubated at 37 ºC for 48 h and then the growth medium was removed and replaced with fresh medium and the cells were further incubated for another 24 h. Sixteen hours before the endpoint of the experiment, 10 μL of AB solution were added to each well. RPMI with 10% AB was used as blank, whereas cells treated with 1% DMSO were used as control. For each condition, including the control conditions, three replicas were prepared. The assay was performed in three independent experiments.

2.7.1. Statistical analysis

Statistical analysis of the cytotoxicity data was carried out using the GraphPad Prims 7.01 software for *Windows*. The results are expressed as a mean and standard deviation obtained from three independent experiments, each comprising three replicate measurements performed for each concentration of each compound tested plus the untreated control. A *p*-value of < 0.05 was considered significant.

3. Results and Discussion

3.1. Synthesis of the complex 1

The reaction of [Ru([9]aneS$_3$)(DMSO)Cl$_2$] with equimolar amounts of sodium methoxide and curcumin in methanol yielded the complex [Ru(II)([9]aneS$_3$)(curcumin)(*S*-DMSO)]Cl (**1**). The complex is microcrystalline and dark red in colour. It was obtained in a fairly good yield (37%), higher than those reported for other ruthenium complexes with *O*-coordinated ligands [42]. It is soluble in polar solvents as DMSO or methanol, but insoluble in water.

10

3.2. Spectroscopic properties

3.2.1. Fourrier-Transform Infrared spectroscopy in the solid-state

The most relevant FT-IR band frequencies of the powdered samples of curcumin and

complex **1** are presented in table 1. The most intense vibrations are associated with the

diketonato group, which is directly coordinated to the ruthenium core atom in complex

1. It must be noted that the 1628 and 1604 cm^{-1} bands have a strong mixed character,

comprising ν(C=C) and ν(C=O) contributions [43]. Nevertheless, a red shift upon metal

coordination was expected, since it was previously observed with curcumin copper

complexes [20]. A combination of stretching and bending modes account for the most

intense spectral band, observed at 1510 cm^{-1} in pure curcumin [43] and at 1508 and

1505 cm^{-1} in complex **1**. Also noteworthy is the observation of a new band at 482 cm^{-1}

in the spectrum of complex **1**, attributed to the Ru–O stretch [44, 45].

3.2.2. UV-vis spectroscopy in solution

The UV-vis absorption spectrum of the complex **1** is dominated by an intense

absorption band in the blue region, with a maximum at 413 nm (in DMF). It is worth

mentioning that pure curcumin peaks at 432, thus meaning that its chelation causes a

hypsochromic displacement of 19 nm in regard to its free form (figure 1a).

The emissive properties of curcumin and complex **1** was assess in DMF at room

temperature and after excitation at 430 nm. The curcumin exhibited a fluorescence

emission dominated by a band centred at 524 nm with a fluorescence quantum yield

(Φ_F) of 0.18 (figure 1b). In contrast, the emission of complex **1** after excitation at the

same wavelength is practically non-existing. The emission of fluorescence in pure

curcumin is a result of the delocalised π-conjugated electronic system and it is strongly

influenced by solvents, tautomerism, and structural modifications [46]. This may

11

explain the lack of fluorescence in complex **1**, since curcumin undergoes a

conformational change in the keto-enol group upon coordination with the metal center.

The occurrence of a similar delocalisation in the organometallic compounds

Ru(arene)(curcuminate)(PTA) (arene = *p*-cymene or hexamethylbenzene) has also

resulted in an absence of fluorescence emission in regard to free curcumin [28].

3.3. NMR

Solution phase NMR determined the structure of complex **1** and geometry of

coordination of the curcuminate ligand, evidencing also that DMSO was kept in the first

coordination sphere (^{1}H and ^{13}C spectra are depicted in Figures S1 and S2, respectively,

of the Electronic Supplementaty Information). Several curcumin proton signals

presented shifts upon coordination, as listed in the table 2 (refer to the scheme 2 for

curcumin atom labelling). Indeed, the H-1 and H-4,4' resonances appeared shielded

when compared with those of free curcumin. This effect resulted from the increased

electronic density and evidences the *O,O*-coordination. The resonances of the aromatic

ring protons were not affected and the signal of the 2'-OH was, as expected, absent.

Regarding the thioether macrocycle, [9]aneS$_3$, the resonances of the methylene protons

appeared as four multiplets at δ 3.66-3.58, 3.42-3.38, 2.93-2.80 and 2.72-2.65 ppm. The

resonances of protons ascribed to the two equivalent methyl groups of coordinated

dimethylsulfoxide appeared as a singlet at δ 2.96 ppm, thus evidencing *S*-coordination

for DMSO.

The 2D NMR experiments (HSQC and HMBC spectra, presented in the

Electronic Supplementary Information) allowed the identification and confirmation of

the carbon resonances. The methoxy carbons (deemed 7,7'-OCH$_3$), the carbons of

coordinated DMSO (deemed S-(CH$_3$)$_2$) and those corresponding to trithiacyclononane

ligand (deemed CH$_2$-[9]aneS$_3$) were confirmed by the $^1J_{C-H}$ HSQC correlations, whereas

the $^{2/3}J_{C-H}$ HMBC correlations allowed the identification of the other carbons. In the ^{13}C

NMR spectrum of the complex **1**, the resonance ascribed to the DMSO methyl groups

appeared at 42.2 ppm and the six methylene carbons of [9]aneS$_3$ appeared at 33.6, 32.1

and 29.5 ppm. The ^{13}C NMR spectrum of the complex **1** also showed the curcumin

carbon resonances, some slightly shifted in regard to the values observed for pure

curcumin (table 3). As expected, the resonances ascribed to C-1 and C-2,2' were the

most affected, suffering shifts of *ca.* 8 and 5 ppm, respectively. Furthermore, the C-4,4',

C-5,5' and C-6,6' also appear shifted.

3.4. Mass spectrometry

The ESI$^+$-MS spectrum of complex **1** (in methanol) showed the most intense peak at *m/z*

727, corresponding to the molecular cation, [Ru([9]aneS$_3$)(curcumin)(DMSO)]$^+$. The

second most intense peak occurred at *m/z* 621, and it corresponds to a fragment

generated by loss of one ethylene unit of the macrocycle along with the coordinated

DMSO, [Ru([9]aneS$_3$–CH$_2$CH$_2$)(curcumin)]$^+$. This fragmentation pattern is typical of

ruthenium(II)trithiacyclononane complexes, as demonstrated by the studies developed

by the group of Santana-Marques [47, 48].

3.6. Photooxydation of 9,10-dimethylanthracene (DMA)

The ability of the complex **1** and curcumin to generate singlet oxygen was assessed by

the 9,10-dimethylanthracene (DMA) photobleaching assay. The DMA is a well-known

singlet oxygen ($^1O_2$) quencher that reacts selectively with $^1O_2$ to form a non-absorbing

endoperoxide derivative [36, 37]. It was observed that DMA photooxidation caused by

curcumin is higher than that caused by complex **1** and lower than the one caused by

5,10,15,20-tetraphenylporphirin (TPP), considered a good oxygen producer. In all cases

the DMA photooxidation follows a first-order kinetic and the observed rate constants

13

(K_{obs}) are given in table 4. The DMA photosensitisation followed the order TPP >>

curcumin > complex **1**. Considering that the reported $^1O_2$ quantum yield (Φ_Δ) of TPP in

DMF is 0.65 [38], the Φ_Δ of curcumin and complex **1** are 0.06 and 0.04 respectively.

Note also that no significant photodecomposition of DMA was detected in the absence

of a photosensitiser.

3.7. Influence of 1 on the thermal denaturation of DNA

This assay provides evidence for the intercalation of small molecules into the DNA

double helix, measurable from the increase of the DNA melting temperature (T_m), *i.e.*,

the mean temperature at which double stranded DNA denatures into single stranded

DNA. The melting curves of salmon sperm DNA (*sm*DNA), either pure or in the

presence of curcumin or complex **1** are shown in figure 2. Under our experimental

conditions, the T_m value of *sm*DNA (100 μM in PBS, see experimental section for

details) was calculated at 84.8 °C. It was not significantly altered by the presence of

curcumin, but in the presence of the complex **1**, at a concentration ratio of

[*sm*DNA]/[**1**]=10 : 1, the melting temperature was higher. The calculated ΔT_m is 7.4 ºC

(table 5), which is indicative of intercalative interaction.

3.8. Cytotoxicity assays

The effect of complex **1**, in comparison with that of curcumin, on the viability of

cultured human prostate PC-3 cells was studied using the Alamar Blue assay. To

establish the safety profile of curcumin and complex **1** they were also incubated with

pre-neoplastic epithelial prostate cells of the PNT-2 cell line. Cells were incubated for a

period of 48 h in RPMI-1640 medium in the presence of curcumin or complex **1** at

concentrations of 20, 50 and 80 μM (figure 3). Given that curcumin is a photosensitive

compound, the manipulation and culture was carried out under reduced light conditions.

14

After 48 h of incubation, the culture media was replaced by fresh media (without compounds).

At the tested concentrations, complex **1** was innocuous against the normal prostate epithelial cells (PNT-2 cell line). However, it also showed no effect on the viability of the cells of the prostate cancer line (PC-3). Such results are somewhat unexpected, given the ability of complex **1** to intercalate with the DNA (section 3.7) and the positive results reported for the Ru(II)(arene)(curcumin) analogues [26–28]. Furthermore, the cytotoxic activity of Ru(II)(trithiacyclononane) complexes was demonstrated on several tumoral cell lines, both human (MG-63, PC-3 and MDA-MB-231) [31, 32], and murine (TS/A) [49]. In particular, [Ru([9]aneS$_3$)(phpz)Cl$_2$] (phpz = 5-(2-hydroxyphenyl)-3-[(4-methoxystyryl)pyrazole]) presented cytotoxic effect against the PC-3 cells (IC$_{50}$ 32.3 μM), though this activity is lower than that of cisplatin (6.6 μM) and free phpz (9.9 μM) against the same cell line [32]. Reduction of ligand cytotoxicity upon coordination to a Ru(II) complex is not infrequent, being also reported for [Ru(II)(*p*-cymene)(curcumin)Cl]) [26] and [Ru(II)(hexamethylbenzene)(curcumin)Cl]) [27]. Lipophilicity was also recently appointed as an important factor for a high cytotoxicity in other Ru(II) curcumin compounds [50]. In this way, using [9]aneS$_3$ macrocycle as the face-capping ligand, instead of the arene, affords complex **1** with a much stronger polar character which may account for the lack of noticeable cytotoxic activity.

4. Conclusions

The complex [Ru([9]aneS$_3$)(curcumin)(DMSO)]Cl (**1**) herein reported is obtained in a good yield with a simple one-pot synthesis. Characterisation using both solution and solid-state techniques, namely elemental analysis, FT-IR, 1-D and 2-D NMR and ESI$^+$-MS, has allowed to unequivocally determine its composition and geometry. Inorganic

15

mononuclear Ru(II) complexes with *O,O'*-donor ligands are rare, and the complex **1**

herein reported is a worthy example of such species. Another fascinating example of

these complexes is [Ru(2,2'-bipyridine)(2-hydroxynicotinate)(dppb)]PF$_6$ [dppb = 1,4-

bis(diphenylphosphino)butane], recently reported by Barbosa et al. as a promising novel

anti-tuberculosis agent [51].

Ruthenium complexes, as mentioned in the introductory section of this work, are

often used to reduce toxicity of active ligands on healthy cells, thus increasing the

selectivity of antitumor compounds. In the case of complex **1**, *in vitro* studies showed

that it does indeed make curcumin innocuous to the normal epithelial prostate cells

(PNT-2 line) but its cytotoxic action is so reduced that it was unable to interfere with

the viability of the tumoural cell line PC-3. Possible causes for this result are the high

photochemical stability of complex **1** and its high polarity. A careful choice of the

spectator and the face-capping ligands, increasing lipophilicity, is the most obvious path

for future developments on this family of complexes.

Regarding complex **1** itself, its polarity and DNA-binding abilities make it

suitable for interfering with the cell lifecycle, providing that it can be conveyed in a

more lipidic carrier to facilitate its cell uptake. A follow-up work will thus include the

encapsulation of this complex into different carriers such as liposomes or solid lipid

nanoparticles, the evaluation of its uptake by different cell types and unicellular

microorganisms, and the study of its potential application as a cytotoxic or biocide

agent.

16

References

1. J. Pelletier, A. Vogel, *J. Pharm*.**I**, 289 (1815).

2. P. R. Holt, S. Katz, R. Kirshoff. *Dig. Dis. Sci.* **50**, 2191 (2005).

3. S. Shishodia, G. Sethi, B. B. Aggarwal. *Ann. NY Acad. Sci.* **1056**, 206 (2005).

4. M. Subramanian, Sreejayan, M. N. Rao, T. P. Devasagayam, B. B. Singh. *Mutat. Res*. **311**, 249 (1994).

5. Sreejayan, M. N. Rao. *J. Pharm. Pharmacol*., **46**, 1013 (1994).

6. M. L. Kuo, T. S. Huang, J. K. Lin. *Biochim. Biophys. Acta* **1317**, 95 (1996).

7. M. Iqbal, S. D. Sharma, Y. Okazaki, M. Fujisawa, S. Okada. *Pharmacol. Toxicol*., **92**, 33 (2003).

8. S. Busquets, N. Carbó, V. Almendro, M. T. Quiles, F. J. López-Soriano, J. M. Argilés. *Cancer Lett*. **167**, 33 (2001).

9. T.-H. Leu, M.-C. Maa. *Curr. Med. Chem. Anticancer. Agents* **2**, 357 (2002).

10. A. Duvoix, R. Blasius, S. Delhalle, M. Schnekenburger, F. Morceau, E. Henry, M. Dicato, M. Diederich. *Cancer Lett*. **223**, 181 (2005).

11. G. Garcea, D. P. Berry, D. J. L. Jones, R. Singh, A. R. Dennison, P. B. Farmer, R. A. Sharma, W. P. Steward, A. J. Gescher. *Cancer Epidemiol. Biomarkers Prev*. **14**, 120 (2005).

12. N. G. Vallianou, A. Evangelopoulos, N. Schizas, C. Kazazis. *Anticancer Res*. **35**, 645 (2015).

13. P. Anand, A. B. Kunnumakkara, R. A. Newman, B. B. Aggarwal. *Mol. Pharm*. **4**, 807 (2007).

14. M. C. Henriques, M. A. F. Faustino, S. S. Braga. *Anti-Canc. Agents Med. Chem.* **17**, in press (2017).

15. S. Banerjee, A. R. Chakravarty. *Acc. Chem. Res*. **48**, 2075 (2015).

16. R. Sareen, N. Jain, K. L. Dhar. *Pharm. Dev. Technol*. **20**, 1 (2015).

17. D. Pucci, A. Crispini, B. S. Mendiguchía, S. Pirillo, M. Ghedini, S. Morelli, L. De Bartolo. *Dalton Trans*. **42**, 9679 (2013).

18. D. Pucci, T. Bellini, A. Crispini, I. D'Agnano, P. F. Liguori, P. Garcia-Orduña, S. Pirillo, A. Valentini, G. Zanchetta, J. Reedijk, D. Pucci. *Med. Chem. Commun*. **3**, 462 (2012).

19. F. Kühlwein, K. Polborn, W. Beck. *Z. Anorg. Allg. Chem*. **623**, 1211 (1997).

17

20. X.-Z. Zhao, T. Jiang, L. Wang, H. Yang, S. Zhang, P. Zhou. *J. Mol. Struct.* **984**, 316 (2010).

21. Z. Pi, J. Wang, B. Jiang, G. Cheng, S. Zhou. *Mat. Sci. Eng. C* **46**, 565 (2015).

22. A. Valentini, F. Conforti, A. Crispini, A. De Martino, R. Condello, C. Stellitano, G. Rotilio, M. Ghedini, G. Federici, S. Bernardini, D. Pucci. *J. Med. Chem.* **52**, 484 (2009).

23. K. H. Thompson, K. Böhmerle, E. Polishchuk, C. Martins, P. Toleikis, J. Tse, V. Yuen, J. H. McNeill, C. Orvig. *J. Inorg. Biochem.* **98**, 2063 (2004).

24. N. Miklášová, E. Fischer-Fodor, R. Mikláš, L. Kucková, J. Kožíšek, T. Liptaj, O. Soritau, J. Valentová, F. Devínsky. *Inorg. Chem. Commun.* **46**, 229 (2014).

25. P. J. Dyson, G. Sava. *Dalton Trans.* 1929 (2006).

26. F. Caruso, M. Rossi, A. Benson, C. Opazo, D. Freedman, E. Monti, M. B. Gariboldi, J. Shaulky, F. Marchetti, R. Pettinari, C. Pettinari. *J. Med. Chem.* **55**, 1072 (2012).

27. L. Bonfili, R. Pettinari, M. Cuccioloni, V. Cecarini, M. Mozzicafreddo, M. Angeletti, G. Lupidi, F. Marchetti, C. Pettinari, A. M. Eleuteri. *ChemMedChem.* **7**, 2010 (2012).

28. R. Pettinari, F. Marchetti, F. Condello, C. Pettinari, G. Lupidi, R. Scopelliti, S. Mukhopadhyay, T. Riedel, P. J. Dyson, "Ruthenium(II)–Arene RAPTA Type Complexes Containing Curcumin and Bisdemethoxycurcumin Display Potent and Selective Anticancer Activity", *Organometallics*, vol. 33, no. 14, pp. 3709–3715, 2014.

29. J. Marques, T. M. Braga, F. A. A. Paz, T. M. Santos, M. F. S. Lopes, *Biometals* vol. 22, pp. 541–556, 2009.

30. J. Marques, T. M. Santos, M. P. M. Marques, S. S. Braga. *Dalton Trans.* 9812 (2009).

31. J. Marques, J. A. Fernandes, F. A. A. Paz, M. P. M. Marques, S. S. Braga. *J. Coord. Chem.* **65**, 2489 (2012).

32. J. Marques, V. L. M. Silva, A. M. S. Silva, M. P. M. Marques, S. S. Braga. *Complex Metals* **1**, 7 (2014).

33. S. S. Braga, J. Marques, E. Heister, C. V. Diogo, P. J. Oliveira, F. A. A. Paz, T. M. Santos, M. P. M. Marques. *Biometals* 27, 507 (2014).

34. S. Revathy, S. Elumalai, M. Benny, B. Antony. *J. Experim. Sci.* **2**, 21 (2011).

35. M. E. Milanesio, M. G. Alvarez, J. J. Silber, V. Rivarola, E. N. Durantini. *Photochem. Photobiol. Sci*. **2**, 926 (2003).

36. B. Stevens, B. E. Algar. *J. Phys. Chem*. **72**, 2582 (1968).

37. R. Castro-Olivares, G. Günther, A. L. Zanocco, E. Lemp. *J. Photochem. Photobiol. A: Chem*. **207**, 160 (2009).

38. J. C. J. M. D. S. Menezes, M. A. F. Faustino, K. T. Oliveira, M. P. Uliana, V. F. Ferreira, S. Hackbarth, B. Röder, T. T. Tasso, T. Furuyama, N. Kobayashi, A. M. S. Silva, M. G. P. M. S. Neves, J. A. S. Cavaleiro. *Chem. Eur. J*. **20**, 1 (2014).

39. G. D. Fasman, Handbook of Biochemistry and Molecular Biology, vol 2 - Nucleic Acids, CRC Press, Cleveland, Ohio, USA, 1975.

40. J. Marmur, *J. Mol. Biol*. **3**, 208 (1961).

41. S. N. Rampersad. *Sensors* **12**, 12347 (2012).

42. J. Marques. Ruthenium(II)-Trithiacyclononane Complexes as Potential Antitumourals. *Dissertation thesis*, Universidade de Aveiro (2013).

43. T. M. Kolev, E. A. Velcheva, B. A. Stamboliyska, M. Spiteller. *Int. J. Quantum Chem*. **102**, 1069 (2005).

44. J. R. Durig, W. A. McAllister, E. E. Mercer. *J. Inorg. Nuclear Chem*. **29**, 1441 (1967).

45. M. Ashok, A. V. S. S. Prasad, V. Ravinder. *J. Brazil. Chem. Soc*. **18**, 1492 (2007).

46. W.-H. Lee, C-.Y. Loo, M. Bebawy, F. Luk, R. Mason, R. Rohanizadeh. *Curr. Neuropharmacol*. **11**, 338 (2013).

47. M. G. O. Santana-Marques, F. M. L. Amado, A. J. F. Correia, M. Lucena, J. Madureira, B. J. Goodfellow, V. Felix, T. M. Santos. *J. Mass Spectrom*. **36**, 529 (2001).

48. R. A. Izquierdo, J. Madureira, C. I. V. Ramos, M. G. O. Santana-Marques, T. M. Santos. *Int. J. Mass Spectrom*. **301**, 143 (2011).

49. B. Serli, E. Zangrando, P. J. Dyson, T. Gianferrara, A. Bergamo, C. Scolaro, E. Alessio. *Eur. J. Inorg. Chem*. 3423 (2005).

50. F. Caruso, R. Pettinari, M. Rossi, E. Monti, M. B. Gariboldi, F. Marchetti, C. Pettinari, A. Caruso, M. V. Ramani, G. V. Subbaraju. *J. Inorg. Biochem*. **162**, 44 (2016).

51.   M. I. F. Barbosa, R. S. Corrêa, L. V. Pozzi, É. O. Lopes, Fe. R. Pavan, C. Q. F.
       Leite, J. Ellena, S. P. Machado, G. Von Poelhsitz,, A. A. Batista, Polyhedron
       85, 376 (2015).

TABLES

Table 1. Selected FT-IR vibrational frequencies (in cm^{-1}) for curcumin and the complex **1** in the solid-state, collected from KBr pellets.

Curcumin	Complex 1	Approximate description
1628	1618	ν(C=C), ν(C=O)
1604	1601	ν(C=C), ν(C=O)
1510	1508, 1505	ν(C=O), δCC10C, δCC=O
—	482	Ru–O

Note: curcumin group band frequencies are described according to the work of Kolev et al. [43]; the Ru–O band is attributed with base on the references [44] and [45].

Table 2. ^{1}H NMR chemical shifts and proton coupling constants of the complex **1** in CDCl$_3$ in comparison with those of free curcumin.

Attribution	Curcumin		Complex 1	
	^{1}H (ppm)	J (Hz)	^{1}H (ppm)	J (Hz)
2'-O*H*	16.07 (s)	—	—	—
H-4,4'	7.60 (d)	15.8	7.30 (d)	16.7
H-10,10'	7.13 (d,d)	8.2 / 1.9	7.10 (d,d)	8.3 / 1.8
H-6,6'	7.06 (d)	1.9	7.01 (d)	1.8

20

H-9,9'	6.94 (d)	8.2	6.94 (d)	8.3
H-3,3'	6.48 (d)	15.8	6.49 (d)	16.7
8,8'-O*H*	5.86 (s)	—	—	—
H-1	5.80 (s)	—	5.64 (s)	—
-OC*H*$_3$	3.95 (s)	—	3.96 (s)	—
-S(C*H*$_3$)$_2$	—	—	2.96 (s)	—
C*H*$_2$-[9]aneS$_3$	—	—	3.66 – 2.65 (m)	—

Note: The TMS signal (0.0 ppm) was used as reference.

21

Table 3. ^{13}C NMR chemical shifts of the complex **1** in CDCl$_3$, in comparison with those of pure curcumin.

Attribution	Curcumin	Complex 1
C-2,2'	183.5	178.3
C-8,8'	148.0	148.6
C-7,7'	146.8	147.5
C-4,4'	140.5	138.0
C-5,5'	127.8	129.2
C-3,3'	123.1	124.5
C-10,10'	121.9	121.9
C-9,9'	115.8	115.4
C-6,6'	114.8	110.4
C-1	109.7	102.2
7,7'-OCH$_3$	56.0	55.1
-S(CH$_3$)$_2$	—	42.2
CH$_2$-[9]aneS$_3$	—	33.6, 32.1, 29.5

Note: The CDCl$_3$ signal (78.76, 78.70 and 78.49 ppm) was used as the internal reference.

Table 4. Kinetic constants for the photooxidation of 9,10-dimethylanthracene (DMA) in DMF by complex **1**, curcumin and TPP.

Photosensitiser	K$_{obs}$(s^{-1})
TPP (reference)	$1.21 \times 10^{-3} \pm 5.01 \times 10^{-5}$
Curcumin	$1.20 \times 10^{-4} \pm 5.29 \times 10^{-5}$
Complex **1**	$6.71 \times 10^{-5} \pm 2.47 \times 10^{-5}$

Table 5. Thermal denaturation values calculated for *sm*DNA and its 10 : 1 mixed solutions with curcumin or the complex **1**.

Sample	T_m (ºC)	ΔT_m (ºC)
*sm*DNA	84.8	
*sm*DNA/curcumin	85.2	0.4
*sm*DNA/**1**	92.2	7.4

22

Figures and schemes
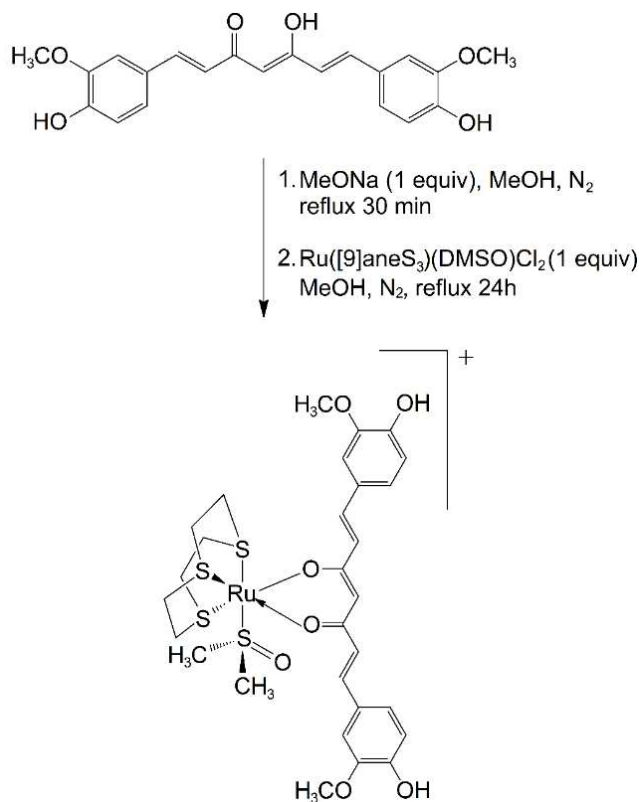
Scheme 1. Reaction scheme for the two-step synthesis of complex **1**.
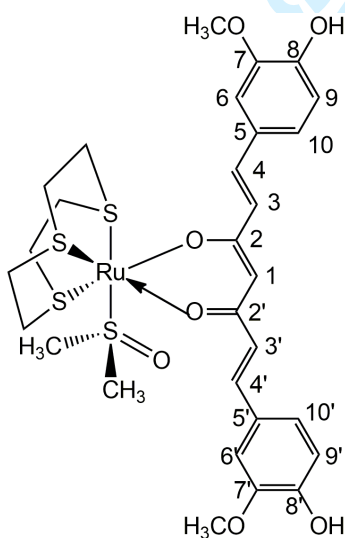
Scheme 2. Structure of the complex **1** depicting the adopted numbering for the carbon atoms of the curcumin fragment..
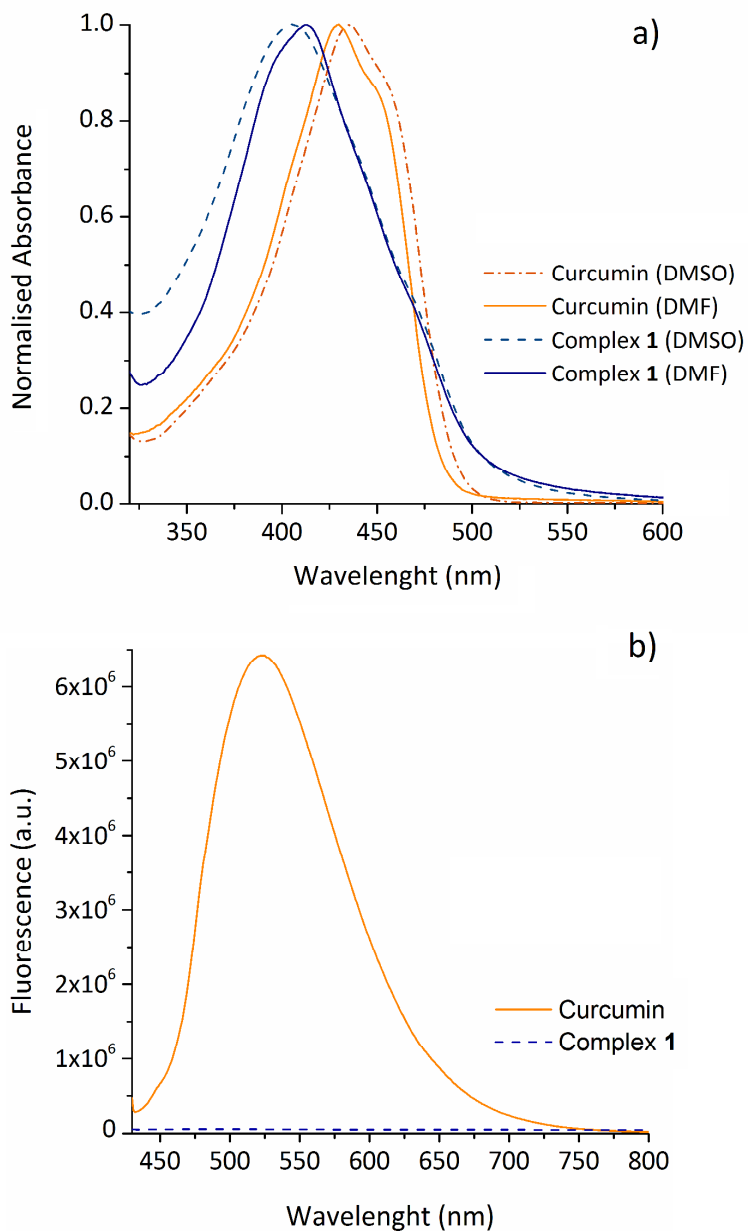
23

Figure 1. Absorption and fluorescence spectra of curcumin and the complex **1** in DMF at ambient temperature: a) the absorption spectra in DMF are normalised and compared with those obtained in DMSO solution; b) the emission spectra were collected following excitation at 430 nm, using a 5 nm slit.

24
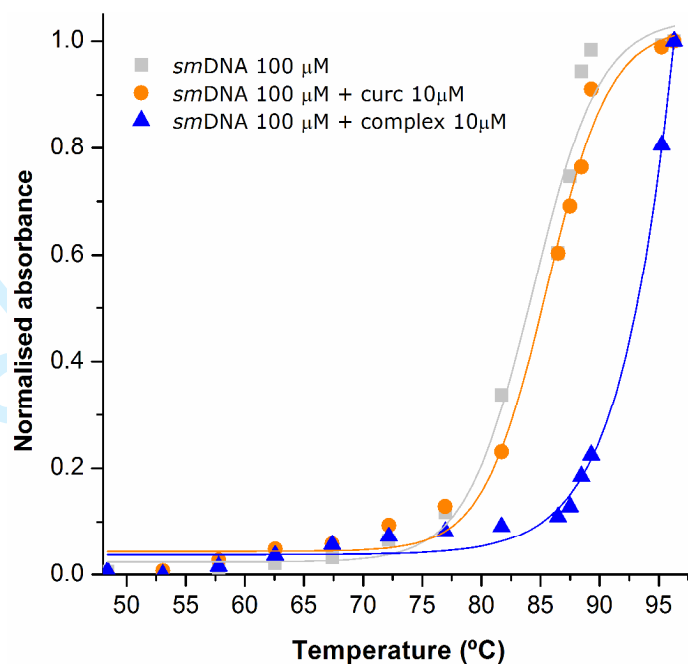
Figure 2. Comparison of the thermal denaturation curves (A_{260} as a function of temperature) for pure *sm*DNA and the mixtures of *sm*DNA/curcumin and *sm*DNA/complex **1** in a 10 : 1 molar ratio. Curves were recorded under equilibrium conditions in PBS (pH 7.2).

25
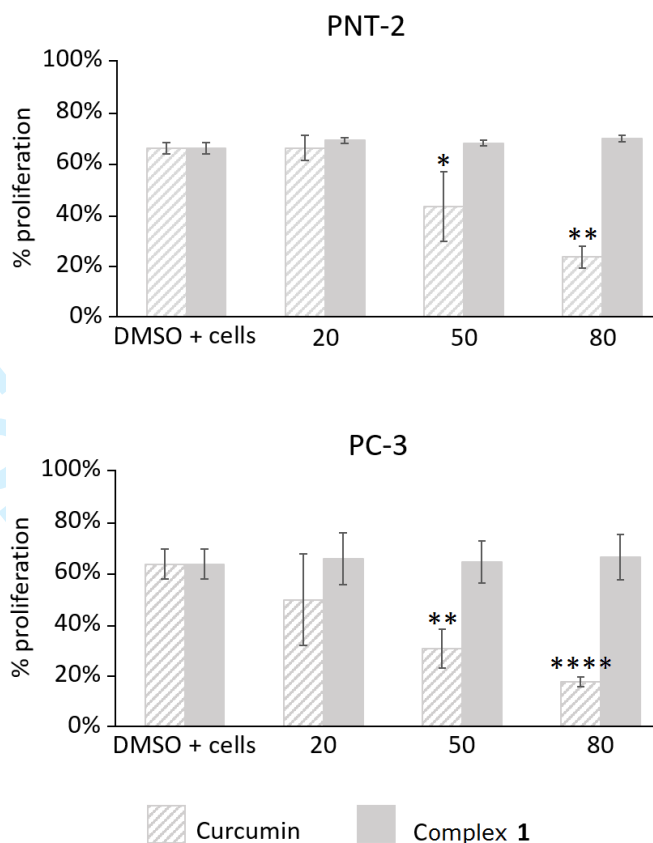
Figure 3. Effect of curcumin and complex **1** on cell viability of PNT-2 and PC-3 cell lines. Cells were kept in the dark at 37ºC and treated for 48 h with different concentrations of curcumin, complex **1** or 1% DMSO (used as vehicle control), as represented in the x-axis. The AB assay was used to determine cell viability. Data are representative of three independent experiments and are expressed as the mean ± SD. *p-value < 0.05, **p value < 0.001 and ****p-value < 0.0001, compared to the group control (DMSO + cells).

26

A ruthenium(II) trithiacyclononane curcuminate complex: synthesis, characterisation, DNA interaction and cytotoxic activity

Magda Carvalho Henriques, Maria Amparo F. Faustino, Artur M. S. Silva, Juliana Felgueiras, Margarida Fardilha and Susana Santos Braga

Electronic Supplementary Information

S1. Extraction and isolation of curcumin.

A crude curcuminoid-rich extract was obtained by stirring 15 g of dry turmeric powder in acetone for 4 h at room temperature. The extract was then concentrated, re-suspended in a 99:1 – dichloromethane:methanol mixture and subject to column chromatography with silica gel (60-120 mesh) as the stationary phase. The first eluent used was dichloromethane to yield fractions with the three curcuminoids and an essential oil (not identified), followed by 99:1 (V/V) dichloromethane/methanol mixture to yield various fractions contaning pure curcumin, with a total volume of roughly 1400 mL. The presence of curcumin in each fraction was verified using TLC (Rf values: 0.49, 0.32, and 0.21 for curcumin, desmethoxycurcumin and bisdesmethoxycurcumin, respectively) and NMR analysis. The saffron yellow curcumin was re-dissolved in a small amount of chloroform and crystalised from a mixture of chloroform/hexane. The purity of curcumin was confirmed by ^{1}H and ^{13}C NMR.

FT-IR ν(tilde) = 3515 m, 3016 m, 2975 m, 2943 m, 2916 m, 2842 m, 1628 s, 1604 s, 1511 vs, 1458 s, 1430 s, 1376 m, 1315 m, 1283 vs,. 1316 s, 1207 s, 1184 s, 1154 vs, 1115 s, 1025 s, 979 m, 962 s, 887 w, 856 m, 815 m, 807 m, 784 w, 745 w, 730 w, 714 w, 621 vw, 601 w, 575 w, 561 w, 542 w, 468 m, 450 w, 398 w, 327 vw, 303 vw, 288 vw.

^{1}H NMR (300.13 MHz, CDCl$_3$): δ (ppm) = 16.07 (1H, s, 2'-O*H*), 7.60 (2H, d, *J*= 15.8 Hz, H4, H4'), 7.13 (2H, dd, *J*= 8.2 Hz, *J*= 1.9 Hz, H10, H10'), 7.06 (2H, d, *J*= 1.9 Hz, H6, H6'), 6.94 (2H, d, *J*= 8.2 Hz, H9, H9'), 6.48 (2H, d, *J*= 15.8 Hz, H3, H3'), 5.86 (2H, s, 8,8'-O*H*), 5.80 (1H, s, H1), 3.95 (6H, s, 7,7'OC*H*$_3$).

^{13}C NMR (75.47 MHz, CDCl$_3$): δ (ppm) = 183.5 (C2, C2'), 148.0 (C8, C8'), 146.8 (C7, C7'), 140.5 (C4, C4'), 127.8 (C5,C5'), 123.1 (C3, C3'), 121.9 (C10, C10'), 115.8 (C9, C9'), 114.8 (C6, C6'), 109.7 (C1), 56.0 (7,7'O*C*H$_3$).

UV-Vis (DMF): λmax (log ε) = 430 nm (104.70). **UV-Vis (DMSO)**: λmax (log ε) = 435 nm (104.68).

S2. 1D and 2D NMR spectra of the complex 1
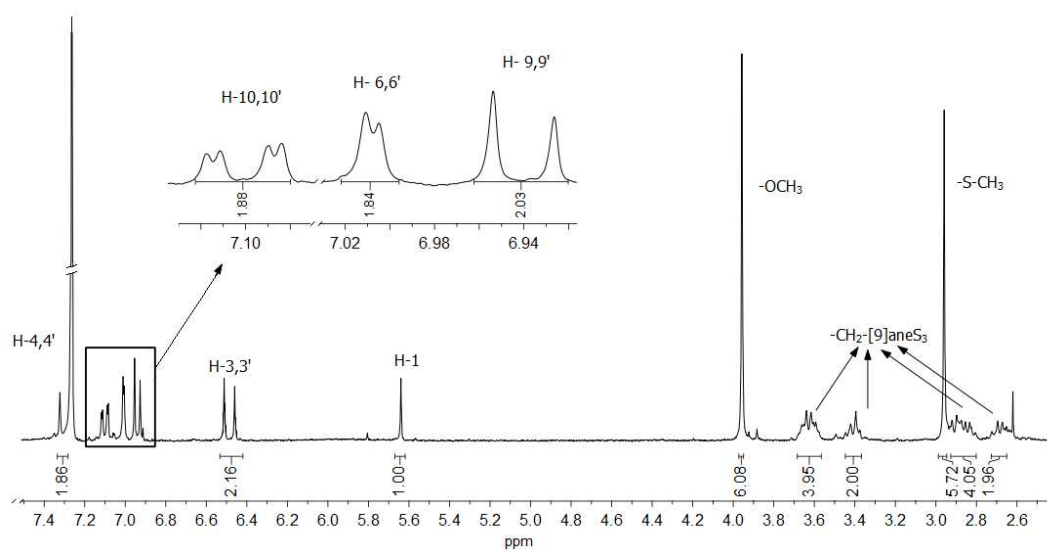
Figure S1: ^{1}H NMR spectrum of the complex **1** in CDCl$_3$
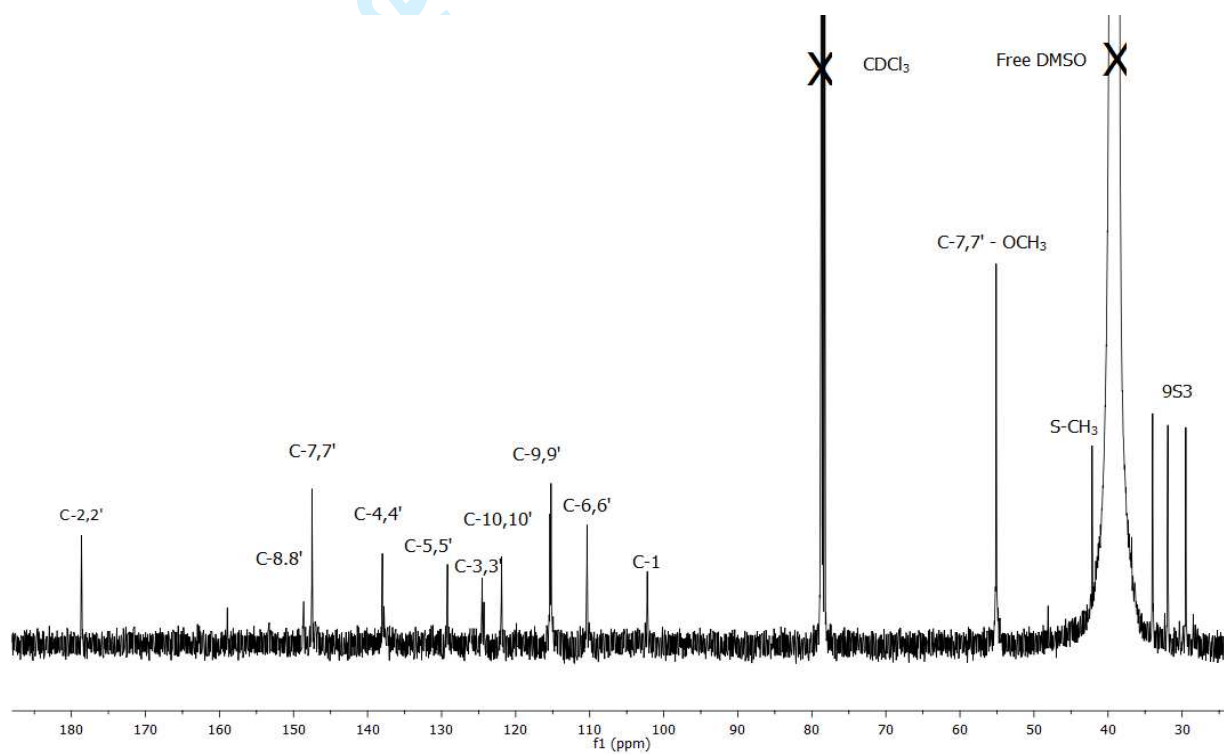
Figure S2: ^{13}C NMR spectrum of the complex **1** in CDCl$_3$. 9S3 denotes the trithiacyclononane macrocyclic carbons. Solvent signals are marked with X.
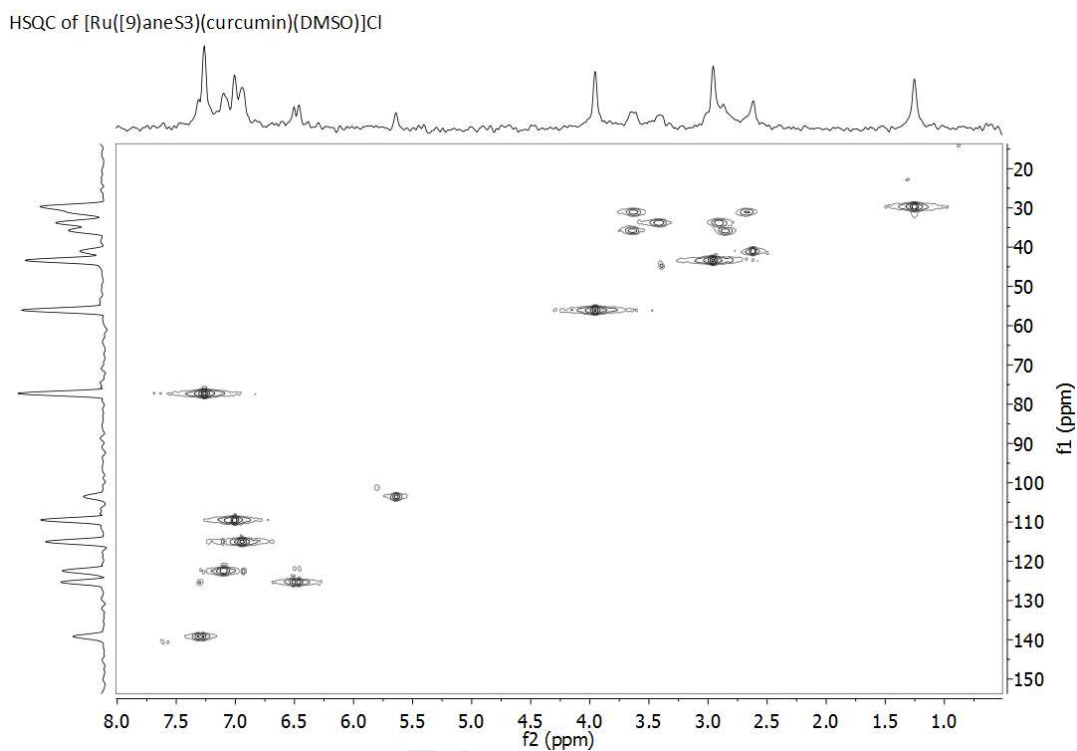
HSQC of [Ru([9]aneS3)(curcumin)(DMSO)]Cl

Figure S3. HSQC spectrum of [Ru([9]aneS$_3$)(curcumin)(DMSO)]Cl (**1**) in CDCl$_3$.

HMBC of [Ru([9]aneS3)(curcumin)(DMSO)]Cl
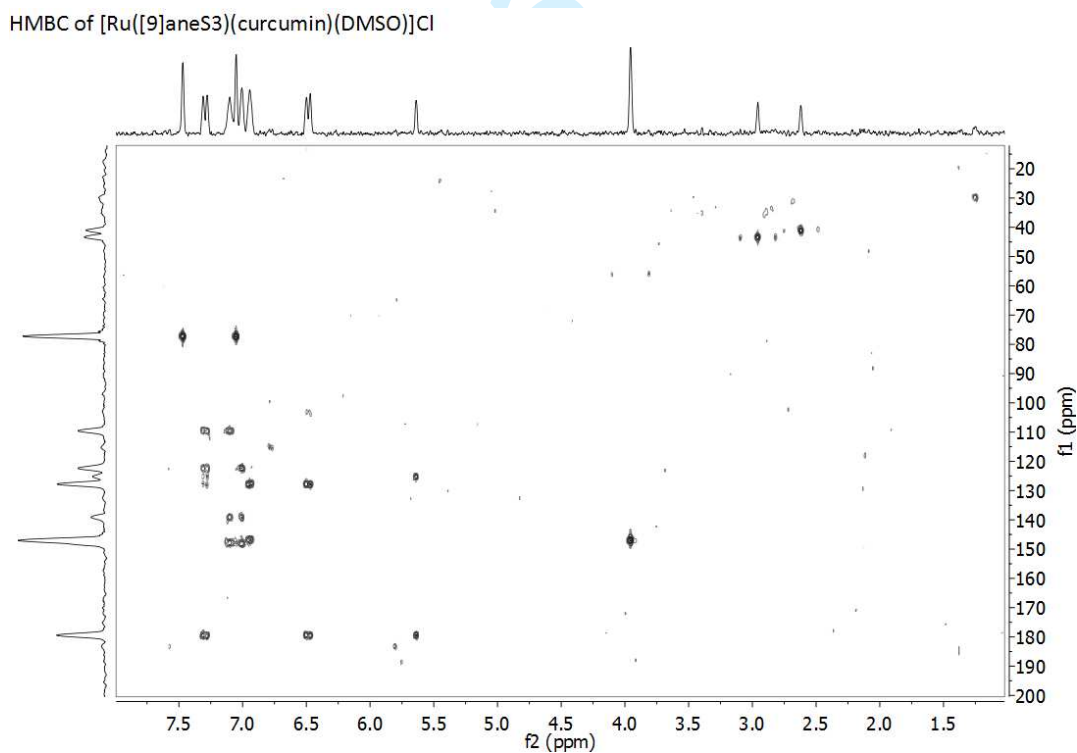

Figure S4. HMBC spectrum of [Ru([9]aneS$_3$)(curcumin)(DMSO)]Cl (**1**) in CDCl$_3$.